Journal of Smart Systems and Stable Energy, 1(3): 208-225 Summer 2022

ORIGINAL RESEARCH PAPER

Multi-objective Optimization of a Micro-turbine and SOFC Hybrid System using Balanced Manta Ray Foraging Optimization Algorithm

Nasser Yousefi

Islamic Azad University, Science and Research Branch, Tehran, Iran

Received: 2021-04-11 Accepted: 2022-06-06 Published: 2022-07-01

ABSTRACT

In this study, economic, environmental, and technical optimization of a hybrid Microturbine-Solid Oxide Fuel Cell (SOFC) system is performed in a full load for the distributed generated electricity. To achieve better results, a new modified metaheuristic, called Balanced Manta Ray Foraging Optimization Algorithm is adopted for multi-objective optimization of the problem. The system has been thermodynamically modeled and the results validated the system efficiency by considering the available data from the reference. During the optimization, the decision variable values have been evaluated by considering the system constraints to achieve an optimal criterion for the cost and exergy efficiency objective functions. Also, the cost of environmental degradation penalty has been added to the system total cost. The effect of the fuel price, investment cost, and the system output power value on the system are taken into consideration. The results show that the most sensitive and the most significant design parameter of the system is the current density of the fuel cell where the accurate selection of it, has a big effect on forming a trade-off between the system cost and the efficiency.

Keywords: *Hybrid system; Micro-turbine; Solid Oxide Fuel Cell (SOFC); Balanced Manta Ray Foraging Optimization Algorithm; exergy analysis; irreversibility; work.*

How to cite this article

Yousefi N. Multi-objective Optimization of a Micro-turbine and SOFC Hybrid System using Balanced Manta Ray Foraging Optimization Algorithm. Journal of Smart Systems and Stable Energy, 2022; 1(3): 208-225.

DOI: 10.52293/SE.1.1.208225

1. INTRODUCTION

With the increase of energy consumption and appearing bad effects of fossil fuels in the environment in the conventional power generation plants, the interesting to some kinds of clean and high efficiency energy generation resources has been increased [1-3]. One of the power generation systems that caught the researchers' attention in recent years is fuel cell [4, 5]. The fuel cell is a kind of power converter that converts the fuel directly into electricity without any pollution and hence, the shortcomings made by combustion are eliminated in this component [6-8]. Also, due to different advantages of fuel cells, such as high efficiency, compatibility with different fuels, and especially, clean energy generation, they count as a trustworthy energy generation resource in the present and the future [9, 10]. Among different types of fuel cells, the Solid Oxide Fuel Cell (SOFC) has several advantages and because of its high operational temperature, it has higher ability to provide more power generation, and higher efficiency based on the output gasses energy [11, 12]. Therefore, by the combination of the SOFCs and a downstream cycle (such as gas turbine), higher efficiency in the range 60% and higher can be provided [13].

Several researches have been performed about hybrid systems[5]; for example, Rossi et al. [14] presented a simplified configuration for dynamic modeling of a hybrid SOFC-Gas turbine system by providing some considerations. Some empirical parameters were employed from operating data to better modeling. The mail purpose was to evaluate degradation efficiency of SOFC during normal

* Corresponding Author Email: *naseryoussefi@yahoo.com*

operations. A practical case study, NETL 430 kW SOFC-Gas turbine is utilized for the method validation. The results showed high agreement between the proposed method and the analyzed system.

Ehyaei et al. [15] proposed a triple cycle including a SOFC, a gas turbine, and steam cycles with an auxiliary burner. The paper analyzed the system based on economic, energy, and exergy points of view. a multi-objective genetic algorithm was utilized for optimizing the triple cycle system. Simulation results indicated that optimal selection of the fuel cell model values increases the exergy efficiency and decrease the generated electricity cost. Also, sensitivity analysis was performed for more considerations.

Habibollahzade et al. [16] suggested a biomass-based fuel/electrolyzer cell for power and hydrogen generation. The suggested system was compared with different gasification agents. The presented combined system was compared in terms of exergy and exergoeconomic terms of view. The system with pure CO_2 was proposed for gasification and was optimized based on multi-objective genetic algorithm. Simulation results showed optimal value for cost and exergy efficiency.

Choudhary et al. [17] proposed a hybrid power cycle by combining a SOFC stack and recuperative gas turbine cycle. The hybrid system was then analyzed based on energy and exergy viewpoints. By applying the parametric analysis, the impact of the inlet temperature of the turbine, the compression ratio, air flow rate, and other parameters were described. The exergy and energy efficiencies of the analyzed system were compared with some works from the literature. The final results indicated high efficiency of the analyzed system.

Ding et al. [18] analyzed the coupling impact of operating parameters on the efficiency of the biogas-fueled SOFC/gas turbine hybrid system. The study analyzed a singular recirculation process based on gas combustor exhaust. The energy and exergy characteristics of the system were analyzed by considering the safety constraints for critical components such as reformer carbon deposition, thermal crack of the SOFC, and steam/carbon ratio. Simulation results showed numerical summarization on coupling impact for numerous operating parameters.

Behzadi et al. [19] proposed a SOFC/GT/Chiller/RO system is presented for power/cooling/fresh water generation. The paper suggested a combined system and analyzed the system in terms of exergy and exergoeconomic viewpoints. For achieving better efficiency, the system was optimized by multi-objective optimization.

Wang et al. [20] presented a hybrid SOFC-GT system united with anode and combustor exhaust recirculation loops. The hybrid system was fueled by a farm biogas. The study investigated parameters optimization and thermal management for the system. The impact of the interaction between the two recirculation loops was conducted in the study. The system efficiency was calculated by the safety constraints. Final results showed that the reasonable fuel and air flow rate, steam to carbon ratio, and fuel utilization comprise the necessary requirement to guarantee the SOFC-GT safety.

The main idea in this research is to give an optimal design and exergy for a CCHP system to achieve Optimal work efficiency, thermodynamic irreversibility, and exergy efficiency [21]. The optimization is made based on a modified model of Manta Ray Foraging Optimization (BMRFO) Algorithm. Another direction of the current research is to consider the environmental considerations of the hybrid micro-turbine and the fuel cell. Generally, increasing the thermal efficiency in the power plants decreases the fuel consumption in which consequently decreases the environmental bad effects (such as CO_2 emission). The fuel cell systems, in contrast to any combustion-based systems, due to its high efficiency and avoiding from the direct combustion of the fuel, presents a cleaner energy. Also, due to high sensitivity of the fuel cell, the input fuel should be purified from the sulfur compounds which prevents from the emission of the sulfuric acid and sulfur oxides in the output gases.

2. SYSTEM MODELING

The overall model for the suggested system is given in Fig. (1). This schematic is a simplified design with considering the most important thermal processes in the conventional system and a combined operation based on SOFC with internal reformer. The system works as follows: the air (point 1) and the fuel (point 9) in the standard environmental condition has been compressed by the compressors and then preheated enough by passing through the preheater and recuperator.

Since only hydrogen can participate in the fuel cell electrochemical reaction, methane gas should be converted into hydrogen during the reforming

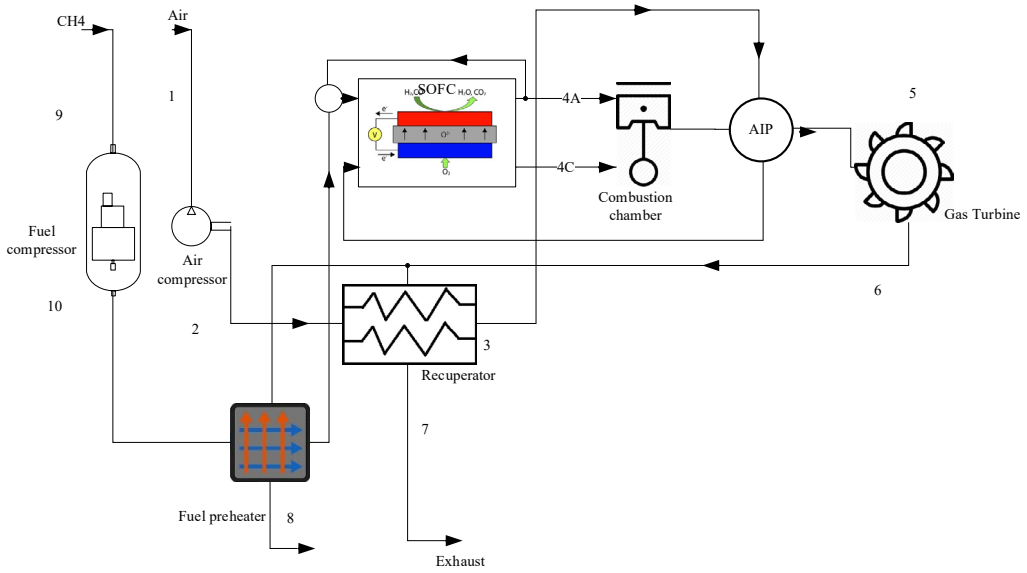

Fig. 1. The schematic of the hybrid power production system based on micro turbine and SOFC

reaction using the high temperature and high-pressure steam. The SOFC configuration with internal reformer is such that the required reactions can be performed in the temperature and the pressure inside the stack. Therefore, the required heat for these reactions will be supplied by the fuel cell electrochemical reaction. Also, it needs to convert a percent of methane into the hydrogen in a pre-reformer before entering to the fuel cell anode. The required steam for the reforming reaction is supplied by returning the products and the steam provided by the electrochemical reaction. This method meets the need for the independent steam generation exchanger. Therefore, to do reforming reaction, the returned products, are pre-reformed with the input methane (point 10) and a part of that, convert the blend into the hydrogen and then, they entered into the anode side of the fuel cell. On the other hand, the oxygen (point 3) enters to the cathode side and the electrochemical reaction has been done on the surface of the electrodes which release a high amount of heat and energy. the output air with flammable ingredients and not consumed fuel (point 4) have been oxidized is a part and release more energy. The hot and high-pressure gasses from the combustion part (point 5) have been expanded for power production in the gas turbine. After expansion (point 6), there is also a high amount of energy that is stored in the gas that most part of it has been recovered by passing through the recuperator for the air pre-heating. About 5% of the output gas from the turbine has been used for pre-heating the fuel. Even, discharged gasses to the environment (point 8) have a little low quality energy for the thermal uses that is not considered in this study.

3. THERMODYNAMIC MODELING

In this study, a steady state model has been adopted for the thermal modeling of the system in the full load condition, which is evolved in each part based on the average values of the thermodynamic parameters [22]. The gradients, temperature and pressure distribution in the fuel cell and other components have been ignored in the calculation and only the output balanced temperature has been considered as the temperature performance of the fuel cell [23]. All of the gasses are assumed ideal and for thermophysical characteristics of the working fluid, the specific heat depends to the temperature degree that is assumed as a polynomial with definite coefficients.

3.1. The compressor and the turbine

For the air and the fuel compressors on one hand, and the gas turbine on the other hand, based on the isentropic efficiency, the determined ratio of the input pressure and the temperature, the gasses output temperature has been achieved the following equations.

$$\int_{T_1}^{T_2} \bar{C}_{p,air} \frac{dT}{T} = \frac{R}{\eta_{AC}} \ln\left(ACPR\right) \quad (1)$$

$$\int_{T_{14}}^{T_{15}} \bar{C}_{p,air} \frac{dT}{T} = \frac{R}{\eta_{FC}} \ln(FCPR) \quad (2)$$

In the present equations, trial and errors are used for estimating the output temperature estimated and after integrating, it is improved to converge to the correct value.

The ratio of the turbine pressure has been evaluated based on the performance pressure and the determined voltage drop values in the system lines. The average value between the input and the output temperatures are utilized for the passed specific heat through the turbine:

$$\int_{T_5}^{T_6} \bar{C}_{p,gas} \frac{dT}{T} = R\eta_T \ln(TPR) \quad (3)$$

$$\bar{C}_{p,gas,avg} \ln\left(\frac{T_6}{T_5}\right) = R\eta_T \ln(TPR) \quad (4)$$

where, TPR describes the turbine pressure ratio.

3.2. Heat exchanger

The bladed plate type has been considered for the recuperator and for modelling the recuperators and the heat exchangers, the *ε-NTU* method is utilized. The heat capacity is used as the average values. Based on the determined value assumed for the performance coefficient, the output temperature from the recuperators is achieved based on the following equation [24]:

$$\varepsilon = \frac{C_h\left(T_{h_1} - T_{h_2}\right)}{C_{min}\left(T_{h_1} - T_{C_1}\right)} = \frac{C_c\left(T_{C_2} - T_{C_1}\right)}{C_{min}\left(T_{h_1} - T_{C_1}\right)} \quad (5)$$

Therefore, evaluating the heat transfer surface of the recuperators is evaluated based on the NTU definition and its equation. For evaluating the Total heat transfer coefficient, the equations from [25] have been utilized.

3.3. Fuel cell with internal reforming

The adopted SOFC in this study is the tube type of it with internal reformer in which its size is extracted from [26]. The model for the fuel cell in this research includes three parts. The internal chemical reactions of the fuel cell is analyzed by using the equilibrium model and the balanced conditions, and the ratio and the molly composition of each gas has been determined in the output composition of the fuel cell. The fuel cell voltage has been evaluated by using the electrochemical model. Eventually, based on energy balance in the fuel cell chamber the temperature and thermodynamic characteristics of the output gasses from the fuel cell chamber have been achieved by considering the input current characteristics and the generated electrical power.

a) Equilibrium model

It is assumed that only the following equations in the SOFC chamber are having flow where among them, reforming and shift reactions are considering in the chemical equilibrium.

$$xCH_4 + xH_2O \leftrightarrow xCO + 3xH_2 Reform \quad (6)$$

$$yCO + yH_2O \leftrightarrow yCO_2 + yH_2 Shifting \quad (7)$$

$$zH_2 + \frac{1}{2zO_2} \leftrightarrow zH_2O Electrochemical \quad (8)$$

where, *x*, *y*, *z* are the molly ratio of the methane reforming reactions, carbon monoxide shifting ratio, and electrochemical ratio, respectively that should be calculated for evaluation the output gasses composition in the fuel cell. However, due to high value of the equilibrium constant of the reform reaction and its high speed in the forward direction, it can be assumed one-directed. This assumption prevents the system equations to achieve extremely nonlinear model. The values of the equilibrium constants using the concentration of the reactants and the products, for the shifting and reforming reactions are given below:

$$K_{P,S} = \frac{P_{CO_2} P_{H_2}}{P_{CO} P_{H_2O}} \quad (9)$$

$$K_{P,R} = \frac{P_{CO} P_{H_2}^3}{P_{CH_4} P_{H_2O}} \quad (10)$$

For evaluating the equilibrium constant of the shifting and reforming reactions, they can be achieved based on experimental equations as polynomial functions (or by minimizing the Gibbs reaction function). In this study, the first method based on [27] is considered:

$$\log(K_P) = AT^4 + BT^3 + CT^2 + DT + E \quad (11)$$

With having the constant value of the equilibrium, and writing the Kinetics equations

based on the molar concentration, and also with determination of the fuel consumption factor in the electrochemical reaction, a system of equations will be produced, in which by solving it, the ratio of all the reactions have been determined.

$$x = n_{CH_4,in} \tag{12}$$

$$K_{P,S} = \frac{\left(n_{H_2,in} + 3x + y - z\right)\left(n_{CO_2,in} + y\right)}{\left(n_{H_2O,in} - x - y + z\right)\left(n_{CO,in} + x - y\right)} \tag{13}$$

$$Z = U_f\left(3x + y\right) \tag{14}$$

where, U_f is the percentage of the fuel consumption.

Consequently, the output gasses moly composition from the anode and the cathode are achieved based on the obtained velocities for the reactions.

Also, the generated electrical current from the fuel cell is achieved by the following equation:

$$I = 2FZ \tag{15}$$

where, F describes the Faraday's constant.

b) Electrochemical model

The fuel cell output voltage evaluation based on the electrochemical model is done by considering the total voltage drops. The ideal (open circuit) voltage of the system has been achieved based in the Nerst equation which is achieved in the system operating temperature and pressure:

$$V_{Nerst} = -\frac{\ddot{A}\bar{g}_f^0}{2F} + \frac{RT}{2F}\ln\frac{P_{H_2}P_{O_2}^{0.5}}{P_{H_2O}} \tag{16}$$

where, $\ddot{A}\bar{g}_f^0$ is equal to the Gibbs function changing of the formation of electrochemical reaction.

Then, the real voltage is achieved after subtracting it with voltage drops related to the Ohmic losses ($\eta_{\dot{U}}$), the activation loss (η_{act}), and the concentration losses (η_{cons}) [23]. Therefore, the formulation of the real voltage is as follows [28]:

$$V_T = V_{Nerst} - \eta_{\dot{U}} - \left(\eta_{act}^{anode} + \eta_{act}^{cathode}\right)\eta_{cons} \tag{17}$$

c) Energy balancing

Energy balancing for the fuel cell stack is determined for evaluating the Enthalpy ratio of the output current based on the determined values of the enthalpy of the input currents to the anode and the cathode, the generated work, and also the total generated pure heat using the internal chemical reactions.

$$H_{in} + H_{react} = W + H_{out} \tag{18}$$

$$H_{react} = -\left(z\Delta h_{el} + y\ddot{A}h_{Shift} + x\ddot{A}h_{Ref}\right) \tag{19}$$

$$H_{in} = \sum n_{j,in}\int_{T_0}^{T_{j,in}} \bar{C}_{p,j}dT \tag{20}$$

$$H_{out} = \sum n_{j,out}\int_{T_0}^{T_{j,out}} \bar{C}_{p,j}dT \tag{21}$$

$$W = IV \tag{22}$$

where, $\ddot{A}h$ describes the pure enthalpy changing ratio for each internal chemical reaction.

d) The combustion section

Assume that the following equations completely happened after exiting from the fuel cell, and by which, the combustible components and the unused fuel in the reaction, have been combined and oxidized with the extra oxygen of the output flow of the cathode to release more thermal energy. To achieve the output temperature, a conventional energy balancing is written to the collection of these reactions and also the input and the output streams of the adiabatic combustion chamber.

$$CH_4 + 2O_2 \rightarrow CO_2 + 2H_2O \tag{23}$$

$$CO + \frac{1}{2}O_2 \rightarrow CO_2 \tag{24}$$

$$H_2 + \frac{1}{2}O_2 \rightarrow H_2O \tag{25}$$

$$\sum_r n_j\left(\bar{h}_{f,j}^0 + \int_{T_0}^{T_{in}} \bar{C}_{p,j}dT\right)\times\varepsilon_c = \sum_p n_j\left(\bar{h}_{f,j}^0 + \int_{T_0}^{T_{out}} \bar{C}_{p,j}dT\right)\times\varepsilon_c \tag{26}$$

where, ε_c signifies the combustion efficiency.

3.4. Problem formulation

Based on the aforementioned relations, the model simulation has been implemented based on MATLAB 2017b environment to model the system

performance based on the designed parameters. Due to complicated relation among different components of the cycle, the direct calculation of the parameters is not possible and because some values such as input temperature to the exchangers are not known at first, these values in the starting have been guessed and then in the continuous iterations of the cycle solution get modified. Therefore, the fuel cell output temperature has been guessed at first, and then based on the presented model, thermodynamic characteristics for all of the cycle points are achieved based on this temperature. These include the temperature of the input flows of the fuel cell [29, 30].

Based on the input Enthalpy and the generated power of the fuel cell, the output temperature in the energy balancing equation has been modified and the calculations have been iterated by the new values of the temperature to converge to the final value. due to the high density of the calculations of the iteration-based method, solving of this system is a time-consuming process and there is a high attempt for decreasing the required computational time in the programming. Such as using the weight coefficients to speed up the solution modification trend in each iteration.

4. EXERGY AND ECONOMICAL ANALYSIS

4.1. Economical modeling

Without considering the economic considerations, the energy system can't be optimized, because the costs are important factors in selection and designing of the energy systems. The optimization of a system only by considering economical or technical considerations can't be a useful solution; because as a general rule, these two objectives are in conflict with each other [31]. The second law of thermodynamics provides a good solution for optimizing this problem [32]. This combination provides a rather new structure for the technical-economic analysis which is called Exergy-economic analysis. The utilized model for the investment cost of the components in the analyzed hybrid microturbine-SOFC system is extracted from [33]. The following equation can be used to transform the investment costs to the cost ratio per unit time:

$$\dot{Z}_K = \frac{C_K \times CRF \times \phi}{N \times 3600} \tag{27}$$

where, C_K signifies the investment cost, or the cost of buying the k^{th} component of the system, CRF describes the return on capital cost that is evaluated based on the annual profit and the time to repay, ϕ represents the operation and maintenance coefficient, and N stands for the number of hours the system works per year [34].

4.2. Exergy pricing

For Exergy analysis using the exergy physical and the chemical relations, the exergy ratio in all of the system lines have been evaluated. The exergy pricing method is based on considering of the exergy economical cost in the system components and establishing the cost balancing equations by the exergy balancing for each of the components [35]. In the cost balancing equation for a control volume (component), the total costs ratio for all of the exergy input and output flows, also the heat and the work exergy, plus the investment and the maintenance cost ratio of that component have been considered.

$$\sum \dot{C}_{in} + \dot{C}_{q,in} + \dot{Z}_K = \sum \dot{C}_{out} + \dot{C}_{w,out} \tag{28}$$

With considering the fuel and the production exergy flows for each component,

$$\dot{C}_{F,K} + \dot{Z}_K = \dot{C}_{P,k} \tag{29}$$

Also, with considering the exergy unit cost,

$$c_f \dot{E}_{F,k} + \dot{Z}_{K,tot} = c_p \dot{E}_{P,k} \tag{30}$$

With considering the fuel and the production exergy flows and using the auxiliary equations, the total cost of balancing equations for all the components, forms a linear equation in which with solving that, the exergy unit cost in all lines of the system has been evaluated. These costs will give useful information about the system performance. The exergy destruction cost rate is the cost that should pay for the thermodynamic inefficiency. The sum of the $\dot{C}_{D,k}$ and $\dot{Z}_K$ indicates consumed cost of each component.

$$\dot{C}_{D,k} = c_f \dot{E}_{D,k} \tag{31}$$

5. OPTIMIZATION

5.1. The Objective Function

To achieve the optimal results for the system decision variables and also making a trade-off between the thermodynamic performance on one hand and the economic and environmental savings

on the other hand, multi-objective optimization is utilized [36-38]. Therefore, the first objective function that should be maximized is the exergy efficiency and is modeled below:

$$F_1 = \eta_{ex,plant} = \frac{w_{net,out}}{m_{CH_4,in} e_{CH_4}} \quad (32)$$

The second objective function is the sum of investment and maintenance rate, operational cost ratio along with the output cost ratio from the CO_2 emissions. The value of the CO_2 emissions has a direct relation with the system efficiency and hence, considering this case in the total objective function increases the weight of the technical criterion compared with the economic criterion.

$$F_1 = \dot{C}_f + \sum \dot{C}_{Cap,O\&M} + \dot{C}_{env} \quad (33)$$

where, the fuel cost per unit of time is determined based on the fuel cost per energy unit. Here, it is assumed 0.004 $/MJ [39]. Also, the cost of environmental penalty is achieved by the following

$$\dot{C}_{env} = c_{CO_2} m_{CO_2} \quad (34)$$

where, c_{CO_2} is considered 0.024 $/kg CO_2 [39].

5.2. Decision variables and the constraints

The decision variables in the present optimization problem are as follows: air compressor pressure efficiency and ratio, input air mass rate, gas turbine efficiency, fuel consumption factor of fuel cell, fuel cell density, recuperator efficiency coefficient, and the steam to carbon ratio in the reformer.

To access to the practical and the feasible results for an optimization problem with practical and physical model, the physical constraints of the problem should be considered in the mathematical model. These constraints are arising from the physical, technological, economical, and the accessibility amount limitations in the market. Table 1 illustrates the applied constraints for the optimization problem.

5.3. Optimization method

Due to the complicated and nonlinear nature of the system, the high amount of decision variables and also the multi-objective nature, a new modified method based on metaheuristics, called Balanced Manta Ray Foraging Optimization Algorithm has been employed.

6. BALANCED MANTA RAY FORAGING OPTIMIZATION ALGORITHM

One of the most amazing aquatic animals is the eagle ray. The body of this animal has smooth surface and millionth forms. These aquatic animals have lived on the planet for about 300 million years. Eagle beams have a cartilaginous skeleton that some scientists classify as the closest sharks. The animal belongs to 18 classes that have different species. The habitat of these animals is open water and freshwater. The animals feed on shellfish, worm, small fish, crabs, or plankton. The largest species of eagle beam is called the Flounder. This species has wingspan of 5 meters. They are very calm and non-toxic animals that feed on plankton. Due to the presence of plankton in the sea, the Flounder usually live in the seas. Due to the tides of the sea waves and the different conditions that occur during the seasons, the population of pathogens decreases, but together they are the main prey of the Flounder. This unique behavior nutritional of the Flounder is interesting to researchers.

Zhao et al. the animal's nutritional behavior has been used in the design of the metaheuristic optimization method that made Manta Ray Foraging Optimization (MRFO) algorithm [41]. The MRFO algorithm obtained satisfactory the result to solve optimization problems. In this investigation, First, a brief explanation of this algorithm is given, then the modified form of MRFO is presented for External Investigation of a HT-PEMFC. The MRFO algorithm has three main concepts for modeling, which are listed below.

6.1. The chain behavior

Based on the chain bait, the Flounders move

Table 1. Optimization constraints utilized in this study [40]

Explanation	Constraint
The constraint of the input temperature to the turbine in the microturbines	$T(5) < 929.85℃$
Maximum operating temperature for the SOFC	$Tcell < 1226.85℃$
Maximum pressure ratio for the single-stage centrifugal compressor	$CPR < 5$
Minimum carbon to steam ratio at reformer	$S/C > 2$

to a location that includes a larger population of plankton, and places, where the plankton population is large, are the most suitable places for the Flounders. Although the most suitable has not been set, the animal is trying to swim to a higher density of plankton, which is possibly the most suitable method to solve the problem.

The swimming of these aquatic animals is head-to-tail to produce a bait chain.

In each iteration, agent update their location based on the most suitable location prey, which is the high population density of plankton.

This behavior nutritional of the Flounder is mathematically expressed as follows.

$$x_i^d(t+1)=\begin{cases} x_i^d(t)+r\times\begin{pmatrix}\left(x_{best}^d(t)-x_i^d(t)\right)\\+\alpha\times x_{best}^d(t)-x_i^d(t)\end{pmatrix}, & i=1\\ x_i^d(t)+r\times\begin{pmatrix}\left(x_{i-1}^d(t)-x_i^d(t)\right)\\+\alpha\times x_{best}^d(t)-x_i^d(t)\end{pmatrix}, & i=2,\ldots,N\end{cases} \quad (35)$$

where, a shows the weight coefficient, Specify the random value and its range is 0 to 1 , $x_{best}^d(t)$ define defines population density of plankton, $x_i^d(t)$ and $x_{i-1}^d(t)$ shows the location of i^{th} and the $(i-1)^{th}$ member at time t in d^{th} dimension, respectively, and α shows a coefficient that expressed as follows:

$$\alpha=2r\times\left|\log(r)\right|^{\frac{1}{2}} \quad (36)$$

6.2. Cyclone behavior

Once the plankton population is determined, the animals form a long bait chain and swim in a spiraling motion toward the bait. based on storm behavior, Flounders swim using two methods: first spiral motion and then swim towards population plankton. The techniques model for storm behavior is obtained below:

$$x_i^d(t+1)=\begin{cases} x_{best}^d+r\times\begin{pmatrix}\left(x_{best}^d(t)-x_i^d(t)\right)\\+\beta\times(x_{best}^d(t)-x_i^d(t))\end{pmatrix}, & i=1\\ x_{best}^d+r\times\begin{pmatrix}\left(x_{i-1}^d(t)-x_i^d(t)\right)\\+\beta\times(x_{best}^d(t)-x_i^d(t))\end{pmatrix}, & i=2,\ldots,N\end{cases} \quad (37)$$

$$\beta=2\exp\left(r_1\times\left(\frac{T-t+1}{T}\right)\right)\times\sin(2\pi r_i) \quad (38)$$

where, T shows the most iteration number, β defines the weight coefficient, and r_1 is the random value and its range is 0 to 1.

During finding the most suitable solution at random, bait is considered to be a reference. In order to find the best random positioning solution, storm behavior is performed to improve the algorithm's exploration.

storm behavior is mathematically expressed as follows.

$$x_{rand}^d=L^d+r\times\left(U^d-L^d\right) \quad (39)$$

$$x_i^d(t+1)=\begin{cases} x_{rand}^d+r\times\begin{pmatrix}\left(x_{rand}^d(t)-x_i^d(t)\right)\\+\beta\times(x_{rand}^d(t)-x_i^d(t))\end{pmatrix}, & i=1\\ x_{rand}^d+r\times\begin{pmatrix}\left(x_{i-1}^d(t)-x_i^d(t)\right)\\+\beta\times(x_{rand}^d(t)-x_i^d(t))\end{pmatrix}, & i=2,\ldots,N\end{cases} \quad (40)$$

where, x_{rand}^d shows random positioning solution, and L^d and U^d defines the minimum and maximum per limitations of the d^{th} dimension, respectively.

6.3. Somersault bait

Based on somersault foraging, the feed position is considered as a pivot. The agent explores for the pivot and somersault to a new location. Therefore, new positions have been considered to achieve the best position. Somersault bait behavior is mathematically expressed as follows:

$$x_i^d(t+1)=x_i^d(t)+S\times\left(r_2\times x_{best}^d-r_3\times x_i^d(t)\right),\quad i=1,2,\ldots,N \quad (41)$$

where, S shows the somersault bait and is equal to 2 and r_2 and r_3 indicate two the random value and its range is 0 to 1.

Following reducing the distance between member's positions, the disorder reduces. As a result, the range of somersault forage decreases with increasing iterations.

6.4. Balanced Manta Ray Foraging Optimization Algorithm (BMRFO)

The Manta Ray Foraging Optimization Algorithm as a new metaheuristic technique has well results for solving the optimization problems, however, in some cases, it faces premature convergence. This section employs two modification mechanisms to improve the algorithm and resolve this issue. The Chaos conception is the first mechanism for modification. This mechanism employs a chaotic map to look forward new positions which have discrete-time dynamical system running in a chaotic state:

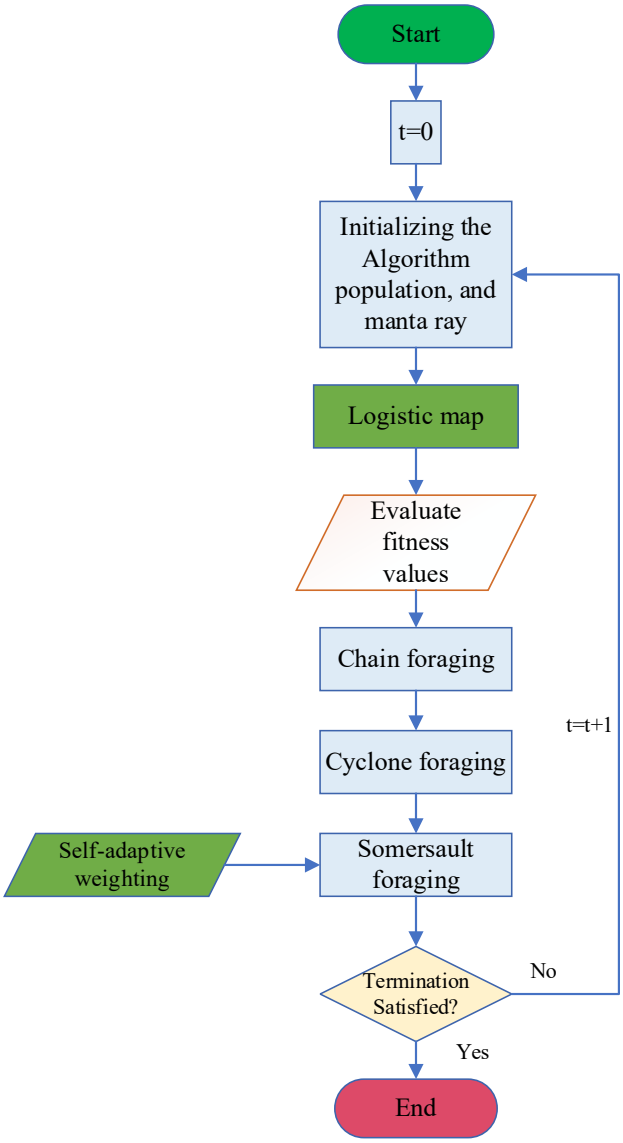

Fig. 2. The flowchart of the BMRFO algorithm

$$\sigma_{m+1} = f(\sigma_m), \quad m = 0,1,2,\ldots \tag{42}$$

In this research, the renown logistic map mechanism is adopted for the chaos implementation. The formulation for this mechanism is as follows:

$$\sigma_{i+1} = \alpha \times \sigma_i (1-\sigma_i) \tag{43}$$

where, i signifies the iteration number, σ_i represents the value for the i^{th} chaotic iteration, α is a coefficient which is considered 4, and the initial value σ_i is considered random value between 0 and 1 [42, 43]. As aforementioned, to generate a chaotic sequence, the chaotic sequence $\sigma_{j,i,q}$ has been formed based on Logistic map, where j represents the generators number in the system, i determines the number of populations, and q represents the iteration number for the algorithm, i.e.

$$\sigma_{j,i+1,q} = 4 \times \sigma_{j,i,q} (1-\sigma_{j,i,q}) \tag{44}$$

Based on this consideration and the carrier wave method, the set of initial variables $x^d_{j,i,q}(t+1)$ is rewritten as follows:

Table 2. The analyzed test functions for the comparison

Function	Formulation	Minimum	Dimension	limitation
Rosenbrock	$f_1=\sum_{i=1}^{D-1}\left\{100\left(x_{i+1}-x_i\right)^2+\left(x_i-1\right)^2\right\}$	0	20	$[-30,30]^D$
Sum Squares	$f_2=\sum_{i=1}^{D} i x_i^2$	0	30	$[-10,10]^D$
Step 2	$f_3=\sum_{i=1}^{D}\left(x_i+0.5\right)^2$	0	30	$[-100,100]^D$
Schwefel 2.22	$f_4=\sum_{i=1}^{D}\lvert x_i\rvert-\prod_{i=1}^{D}\lvert x_i\rvert$	0	30	$[-10,10]^D$
Schwefel 1.2	$f_5=\sum_{i=1}^{D}\left(\sum_{j=1}^{i} x_j\right)^2$	0	30	$[-100,100]^D$
Chung Reynolds	$f_6=\left(\sum_{i=1}^{D} x_i^2\right)^2$	0	30	$[-100,100]^D$

Table 3. The comparison results of the algorithms

Algorithm		f_1	f_2	f_3	f_4	f_5	f_6
GSA [44]	Min	16.4637	0.0009	0.0015	14.0947	0	2.3281e-7
	Max	7.3461e+3	2.2010e+2	1.1930e+5	0.7425e+3	1.0093e-6	1.0849e+9
	Mean	2.7618e+3	7.4183e+2	2.7149e+4	51.2963	8.5749e-8	1.6751e+8
	std	3.3551e+4	3.3323e+2	3.7455e+4	19.5109	3.3728e-7	3.1992e+8
KH [45]	Min	35.0751	0.3116	3.1754	4.2419	3.2419e-6	5.4963
	Max	435.7592	1.3088	6.1852	48.4235	0.0025	105.9062
	Mean	137.2185	1.5190	5.3428	24.2617	0.0010	21.6728
	std	88.4935	0.1185	2.5427	7.2563	0.0007	11.4937
CSA [46]	Min	8.1948	3.3491e-5	5.9068e-5	0.0548	4.0245e-13	7.8206e-9
	Max	6.5982e+2	0.0529	0.0039	0.1108	2.2934e-8	8.2916e-8
	Mean	119.2749	0.0068	0.0019	0.0298	2.7649e-9	3.1145
	std	289.1656	0.0396	4.4913e-5	0.0681	2.5142e-9	2.8061e-8
PF[47]	Min	5.7345	10.4965e-21	4.4127e-11	5.4219e-15	4.7319e-7	4.3452e-38
	Max	49.3492	5.2957e-19	4.2951e-10	3.7234e-14	0.0086	3.2719e-34
	Mean	8.0195	2.3467e-19	2.2437e-10	2.2491e-14	8.4925e-5	2.1860e-35
	std	5.3156	1.0419e-19	8.3195e-11	7.4763e-15	0.0041	6.4958e-35
IPF	Min	6.7041	3.2649e-5	6.3013e-9	0.0019	3.3541e-16	4.3467e-17
	Max	419.0012	2.2538	1.0452e-8	3.3429	0.4602e-12	3.6037e-16
	Mean	65.4106	0.5709	2.5133e-8	0.3122	2.3084e-13	2.1923e-16
	std	87.1596	0.4635	3.6653e-9	0.6567	3.4472e-13	6.4035e-17

$$x_{j,i,q}^{d}=x_{j,i,q}^{min}+\left(x_{j,i,q}^{max}-x_{j,i,q}^{min}\right)\times\sigma_{\mathrm{j,i,q}} \tag{45}$$

where, $x_{j,i,q}^{max}$ and $x_{j,i,q}^{min}$ are the upper and the lower limits of j^{th} the generator is given by forming capacity limits.

The next mechanism is to employ self-adaptive

weighting. This mechanism speeds up the algorithm convergence. The idea is to modify the individual's position to give direction to the random values. This method makes a good trade-off between the local and the global searching. This causes that in the initial steps of the algorithm, the individuals swim with higher step size, and at the last steps, the step size has been reduced by a local search in the search space. This mechanism has been applied to the somersault bait as follows:

$$X_i^d(t+1)=\begin{cases} x_i^d(t+1)=x_i^d(t)+S\times\left(r_2\times x_{best}^d-r_3\times x_i^d(t)\right) \\ +\left(x_{best}^d-x_i^d(t)\right)\times\tau,\ \ rand>0.5 \\ x_i^d(t+1)=x_i^d(t)+S\times\left(r_2\times x_{best}^d-r_3\times x_i^d(t)\right) \\ -\left(x_{best}^d-x_i^d(t)\right)\times\tau,\ \ rand\le 0.5 \end{cases} \quad (46)$$

where,

$$\tau=\begin{cases} \left(\dfrac{f\left(x_{best}^d\right)}{f\left(x_{worst}^d\right)}\right)^2, if\ \ f\left(x_{worst}^d\right)\neq 0 \\ 1 \qquad\qquad\quad , if\ \ f\left(x_{worst}^d\right)=0 \end{cases} \quad (47)$$

where, $f\left(x_{best}^d\right)$ and $f\left(x_{worst}^d\right)$ determine the best and the worst results of the objective function for the individuals, respectively. The mechanism modifies the weight of the algorithm for the hunting behavior to decrease the difference between the worst and the best solutions [38].

6.5. Algorithm validation

To verify the suggested BMRFO algorithm, six test functions are utilized. The results for the functions have been compared with Gravitational Search Algorithm (GSA) [44], Krill Herd (KH) [45], Crow Search Algorithm (CSA) [46], and the basic MRFO [41] to clarify the superiority of the suggested algorithm. Table 2 illustrates the analyzed test functions for the comparison.

Table 3 illustrates the comparison results of the algorithms. Four statistical indexes including Median value, standard deviation value (Std), minimum value and the Maximum value are employed for the algorithms' verification that are achieved by 30 independent runs.

It can be observed that employing the suggested BMRFO gives the minimum value for the test functions. Besides, the results specify that that the proposed BMRFO algorithm has more accuracy than the other compared algorithms in the employed test functions. The results also indicated that the suggested method gives the minimum standard deviation value for the optimized BMRFO algorithm which indicates its higher robustness than the other compared algorithms.

7. CASE STUDY

For applying the suggested optimization strategy on a specific hybrid system, the case study presented in [48] has been employed. In the considered reference, this system is modeled and analyzed in part-load and full load without optimization. The designing and the components parameters of the system is similar to the designed hybrid gas turbine-fuel cell in [49-51]. The studied system has 260 kW output power. The output power is considered constant here. The input air mass rate is considered 0.5 kg/s, and the compressor pressure ratio is assumed 3.8. the fuel cell density is considered 3500 A/m^2 and the fuel consumption percent is 0.80. Also, the carbon to steam ratio is assumed 1.8. The other required parameters in the basic mode are considered as the aforementioned references. CRF is considered 18%, ϕ is assumed 1.08, and N is 8000.

8. RESULTS AND DISCUSSIONS

8.1. System validation and optimization

For validation of the method, the results of the suggested strategy are compared with the results from [49]. The obtained results of the presented model in this research for the identical input parameters are too close to the desired values as can be observed from Table 4. The difference in the output power of the microturbine can be due

Table 4. The comparison results of the simulation

Parameter	Desired value	Model value	Reference [49]
Cell Voltage (V)	0.6	0.6	0
Operational temperature of the fuel cell (℃)	985	982	0.28
Input temperature of turbine (℃)	890	892	0.18
Pure output power of microturbine (kW)	38.54	45.5	12
Pure output power of fuel cell (kW)	218.49	201	6
Thermal efficiency	54.5	56.7	2.8

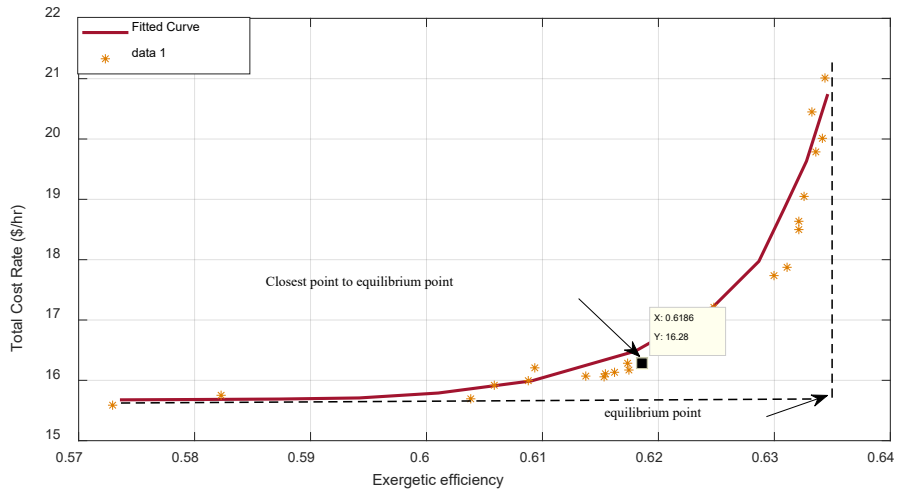

Fig. 3. The distribution profile of the two-objective optimization solutions

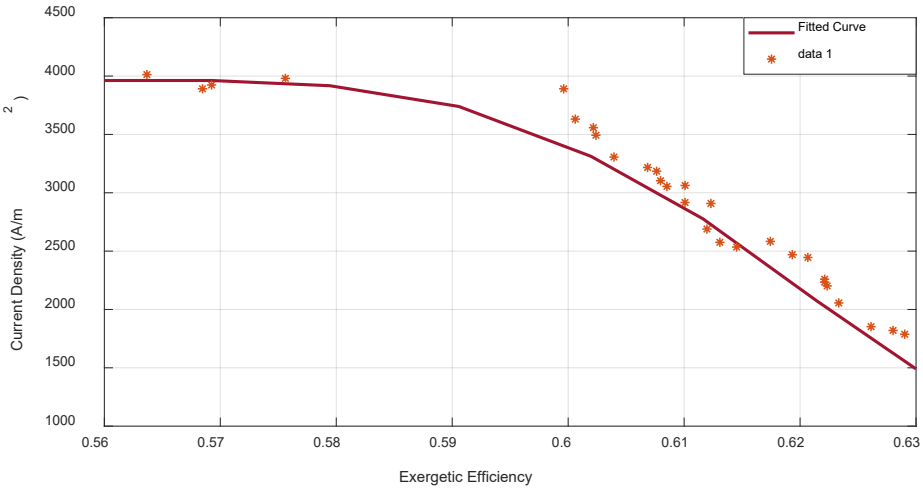

Fig. 4. The density distribution in the obtained solutions range of the pareto profile.

Table 5. The comparison of the optimal state with the initial state

Parameter	Initial state	Optimal state	Percentage of difference
Exergy efficiency (%)	55.49	58.55	5.22
Thermal efficiency (%)	58.94	61.44	4.06
Total cost ratio ($/hr)	15.12	14.87	1.65
C_{env} ($/hr)	1.48	1.43	3.37
T_{clell} (K)	1248	1201	3.77
TIT (K)	1153	1095	5.03

to considering the consumption work of the fuel compressor in the model.

As aforementioned, the optimization problem in this research is to optimize two functions simultaneously to maximize the exergy efficiency and to minimize the total system cost. Because these two objectives are in conflict, the problem has a set of solutions close to the optimal for

Table 6. The design parameters values for both initial state and the optimal state

Component	$E_D\,(kW)$		$E_D / E_{D,tot}\,(\%)$		$C_D\,(\$/hr)$		$f = Z/(Z+C_D)$	
	Initial	Optimized	Initial	Optimized	Initial	Optimized	Initial	Optimized
AC	14	9.5	11.35	8.64	0.29	0.19	0.6	0.65
GT	6.67	6.98	5.7	6.6	0.12	0.13	0.86	0.85
SOFC	48.59	34.61	39.8	39.89	0.43	0.38	0.82	0.85
CC+AIP	38.43	42.6	30.7	30.48	6.15	4.93	0.05	0.08
REC	3.88	3.35	3.5	3.9	0.09	0.07	0.38	0.36
Total	111.57	97.04	91.05	89.51	7.08	5.7	2.71	2.79

Table 7. The design parameters variations toward the investment costs

Parameter	$C_{cap} = 150\%$	$C_{cap} = 100\%$	$C_{cap} = 50\%$
ACPR	4.32	4.32	4.23
η_{AC}	0.66	0.69	0.69
$m_{air,in}\,(\mathrm{kg/s})$	0.27	0.27	0.27
η_{GT}	0.69	0.67	0.64
S/C	0.68	0.66	0.65
ε_{rec}	0.74	0.74	0.69
$i\,(\mathrm{A}/m^2)$	2671	2344	1875
U_f	2.21	2.59	2.49

different values of the corresponding cost and thermodynamic performance. It is obvious that with more decreasing of the exergy destruction ratio, the thermodynamic performance and the system investment cost have been increased. Fig. (3) indicates the total obtained solutions (pareto front) for the system. In this figure, the rate of exergy efficiency changing (technical criterion) in contrast to the system cost ratio (economical criterion) is considered based on $\$/hours$. It can be observed that the best solution is achieved in (0.6186, 16.28).

It can be observed that all the obtained points in the pareto diagram indicate optimal solutions for the system and selecting each of them, depends to the degree of importance of the cost objectives and thermodynamic performance for the system designer. In this paper, for achieving the proper point from the set of solutions for the pareto profile, the equilibrium point method is employed. This hypothetical point is the intersection of the optimal limit for each of two objectives [52].

The closest point on the pareto profile to the equilibrium point is the best solution among the optimal values. By analyzing the distribution values of the design parameters in the obtained solutions range of the pareto profile, it can be considered that the density of the fuel cell has the most effects on the economical and the technical objectives. The other parameters remain constant in almost their optimal range. This behavior is because of that the cost for the fuel cell includes the largest part of the system cost. In other hand, exergy destruction in the fuel cell has direct relation with the density increasing. Also, the maximum rate of the energy conversion happens in the fuel cell and by increasing the density, the value of the exergy destruction and also the irreversibility of the system have been increased. Fig. (4) indicates the density distribution in the obtained solutions range of the pareto profile.

Therefore, the density of the fuel cell can be considered as the most important designing parameter in this system where its optimal value selection is too effective for making a proper trade-off between the cost and the system performance.

Table 5 illustrates the system dependent parameters values, including exergy efficiency, the of the first law efficiency, the system total cost ratio, and the generated carbon dioxide for the initial state of the system, and compared the results from the multi-objective optimization.

The results of the above Table are achieved based on the optimal obtained points from Fig.

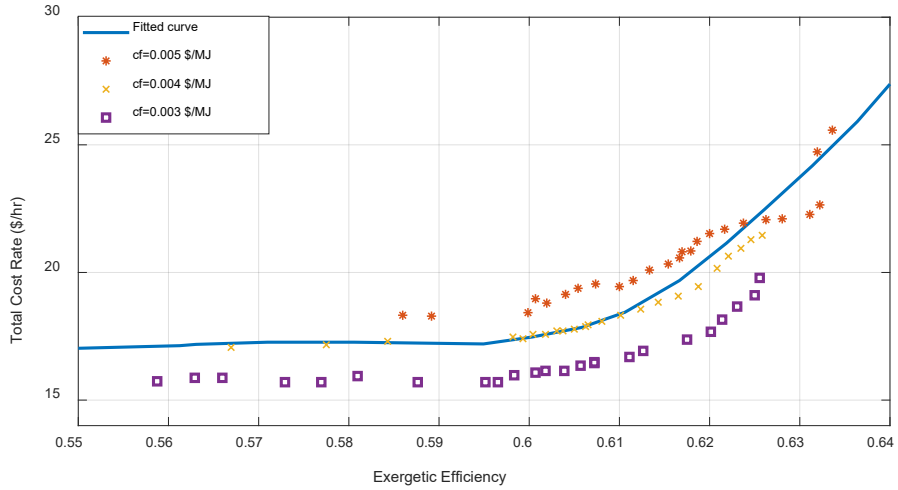

Fig. 5. The results of sensitivity analysis for the changes of the fuel unit cost

(3) that is explained in the before. As can be observed from the results, optimization increases the exergy performance by 5.22% and decreases the environmental penalty cost ratio by 3.37%. While, the total cost ratio has been reduced by 1.65%. Therefore, it can be observed that the initial state which is given in [49], is closer to the optimal value. Table 6 indicates the design parameters values for both initial state and the optimal state.

As can be observed, the maximum changes for the pressure ratio increasing, is the decreasing of the input air mass ratio and the decreasing of the density of the fuel cell. Also, from the Nernst equation, it is clear that the system pressure increasing has a direct relation with the irreversibility decreasing and the fuel cell exergy efficiency increasing.

Also, increasing the compressor pressure ratio increases the turbine pressure ratio and decreases the output gasses temperature. Therefore, temperature reduction of the input hot gasses to the recuperator decrease the input air temperature of the fuel cell, and consequently the need for extra air for the cooling has been decreased. Besides, the amount of carbon to steam ratio for anode re-circulation has been increased to 2.60. Some of the important exergy-economy parameters are given in Table 7.

As can be observed from the results, due to high value of the initial state density, the maximum valye of the exergy destruction happens in the fuel cell.

After that, the most inefficient component is the combustion part such that due to irreversibility reaction in it, and also low performance coefficient of the air injection tubes in the fuel cell, has the maximum exergy destruction value. With reducing the current density to the suggested value in the optimization, the exergy destruction value in the fuel cell has been also decreased. The exergy economical coefficient f, is a significant thermoeconomic parameter which indicates the total investment cost sharing ratio to the consumption cost in a component of the system.

8.2. Sensitivity analysis

To provide a broader vision in the present problem, sensitivity analysis has been applied to the system by changing some constants and parameters. Here, the sensitivity analysis of the pareto profile results is applied by changing the fuel cost and also the initial costs. In Fig. (5), the pareto profile changes is shown with increasing and decreasing of the fuel unit price. The optimization in the basic mode of the fuel unit price is iterated with $C_f = [0.004, 0.003, 0.005]\ \$/Mj$. It is observed that with increasing the fuel cost, the optimal solutions range for the system provide better thermodynamic performance (exergy efficiency increasing). This is due to increasing of the fuel cost effect in the objective function and the total cost. Also, the solutions sensitivity to the fuel cost changes has been decreased by moving into the right side of the diagram. In low efficiencies, due to higher share of the economical objective function toward the exergy efficiency objective function, the sensitivity is more specifically for the fuel cost variations. Also, it can be note that the fuel consumption value has been decreased by increasing the system efficiency and the investment

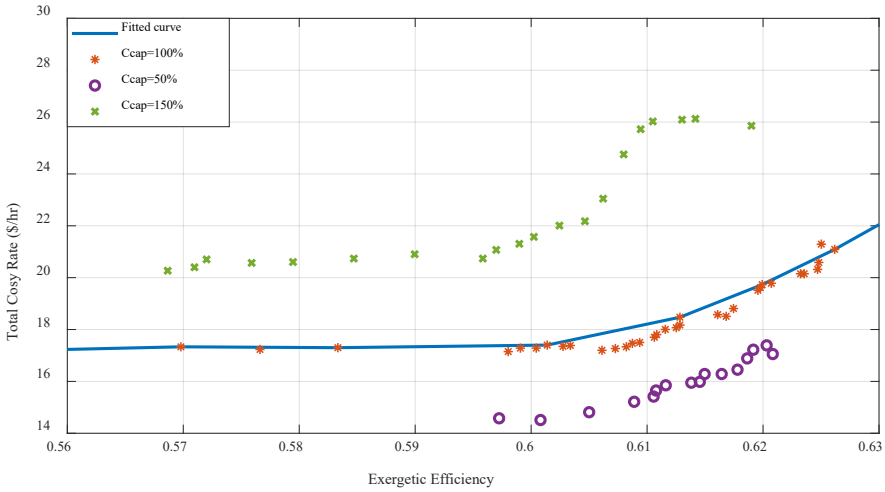

Fig. 6. The results of sensitivity analysis for the changes of the investment cost

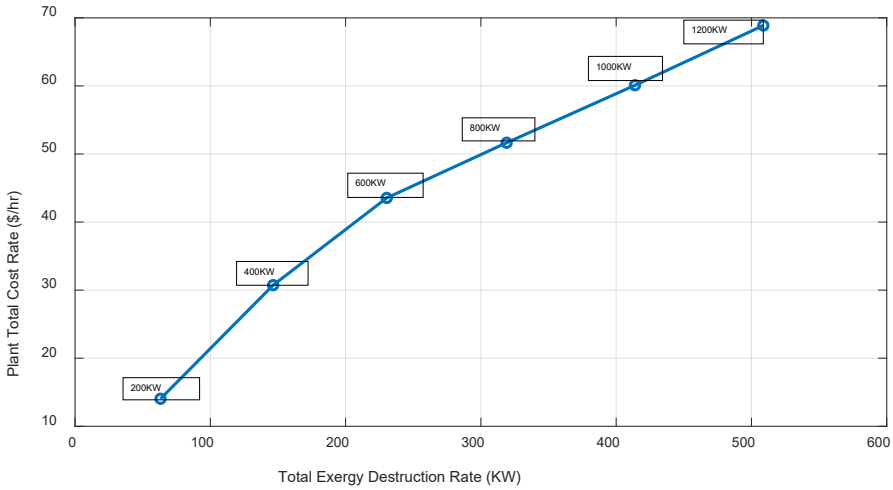

Fig. 7. The optimal value changes for the objective functions (the total cost and the exergy destruction ratio) with the system output power.

cost. As mentioned in the optimization subsection, in balance changing between the effect of the economical objective functions and efficiency, the current density has the most changes to keep the balance between the two objective functions in a better way. Therefore, it can be said that the other parameters rather than the fuel cost change, have not a clear sensitivity. The Pareto profile changes with increasing the and decreasing of the investment costs and buy components is given in Fig. (5).

However, for analyzing the sensitivity of the design parameters to the investment costs, the changes of these parameters for three points of the solutions (C_{cap} =[150%,100%,50%]-Fig. (6)) in which have almost identical exergy efficiency close to the balance point are investigated in Table 6. The results indicate that most of design parameters, except the current density of the fuel cell during the investment cost increasing has not high changes. The current density is the most significant parameter in effecting on the objective function. This parameter, with increasing of the investment cost (increasing the economical objective function), has been decreased, i.e. the optimal design should be change into a better thermodynamic effectiveness to spend less fuel consumption cost.

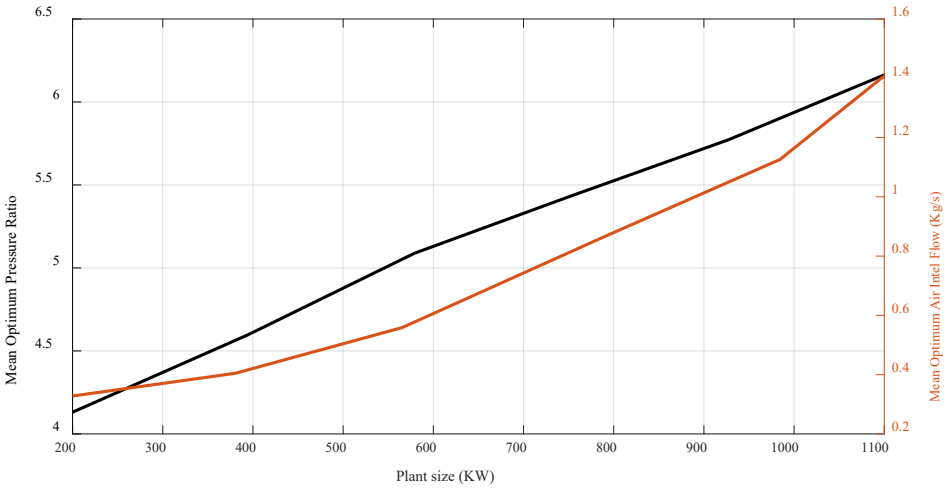

Fig. 8. The optimal values changes for the design parameters

8.3. The changes in the output power or the system scale

To analyze the effect of the scale changes or the output power changes of the system, the optimization is performed to the systems with generated power of 200 kW to 1200 kW. The balance point has been selected from each set of the pareto solutions for each system size and the total cost ratio based on exergy destruction for the selected points are shown in Fig. (7).

It can be considered that with increasing the output power of the system, the cost increasing ratio for each kW generated power has been reduced. It is concluded that for the design parameters variations with system size increasing, most of them have not changes and so, the optimal design parameters values are not sensible to the output power of the system. About the input air mass rate, with increasing the system size, it is clear that the need for the cooling air and naturally, oxygen, has been increased with increasing the input fuel. Also, the optimal range of the compressor pressure due to the increasing of the input air mass rate will be increased in the microturbine. The optimal values changes for the design parameters are shown in Fig. (8).

9. CONCLUSIONS

In this study, a hybrid microturbine- Solid Oxide Fuel Cell (SOFC) system was simulated. The optimal value of the design parameters for a sample system with different output power values are achieved based on a developed design of a metaheuristic, called Balanced Manta Ray Foraging Optimization Algorithm. Two objective functions including exergy efficiency and system total cost were analyzed. Also, the cost of the environmental destruction was added to the analysis and the simulation results contained some points with corresponding values of the exergy efficiency and the system total cost. The simulations indicated that among different designing parameters, the current density of the fuel cell has a specific importance and has an important role for making the balance between both technical and economical purposes. Besides, this parameter is sensitive to the fuel cost changes and the investment cost changes, while the other parameters have not much changes. in analyzing of different sizes of the output power, it was determined that the ratio of the pressure and the input air mass rate were increased by increasing the system size, while the other parameters are constant in their optimal values.

NOMENCLATURE

$\dot{C}$	Cost rate
CPR	Compressor pressure ratio
E	Exergy rate
F	Faraday constant
H	Thermal rate
h	Enthalpy
I	Current
i	Current density

K_P	Fixed chemical equilibrium
m	Mass flow rate
η	Electrical losses
n	Molar flow rate
P	pressure
R	Gas constant
S/C	Carbon to vapor ratio
T	Temperature (K)
TPR	Turbine pressure ratio
U_f	Percentage of fuel consumption
V	Voltage
W	Power
ε	Performance coefficient

REFERENCES

1. Aghajani, G. and N. Ghadimi, *Multi-objective energy management in a micro-grid.* Energy Reports, 2018. **4**: p. 218-225.
2. Akbary, P., et al., *Extracting appropriate nodal marginal prices for all types of committed reserve.* Computational Economics, 2019. **53**(1): p. 1-26.
3. Alizadeh, E., et al., *Investigation of contact pressure distribution over the active area of PEM fuel cell stack.* International Journal of Hydrogen Energy, 2016. **41**(4): p. 3062-3071.
4. Tian, M.-W., et al., *New optimal design for a hybrid solar chimney, solid oxide electrolysis and fuel cell based on improved deer hunting optimization algorithm.* Journal of Cleaner Production, 2020. **249**: p. 119414.
5. Fei, X., R. Xuejun, and N. Razmjooy, *Optimal configuration and energy management for combined solar chimney, solid oxide electrolysis, and fuel cell: a case study in Iran.* Energy Sources, Part A: Recovery, Utilization, and Environmental Effects, 2019: p. 1-21.
6. Mirzapour, F., et al., *A new prediction model of battery and wind-solar output in hybrid power system.* Journal of Ambient Intelligence and Humanized Computing, 2019. **10**(1): p. 77-87.
7. Nejad, H.C., et al., *Reliability based optimal allocation of distributed generations in transmission systems under demand response program.* Electric Power Systems Research, 2019. **176**: p. 105952.
8. Shamel, A. and N. Ghadimi, *Hybrid PSOTVAC/BFA technique for tuning of robust PID controller of fuel cell voltage.* 2016.
9. Gollou, A.R. and N. Ghadimi, *A new feature selection and hybrid forecast engine for day-ahead price forecasting of electricity markets.* Journal of Intelligent & Fuzzy Systems, 2017. **32**(6): p. 4031-4045.
10. Hamian, M., et al., *A framework to expedite joint energy-reserve payment cost minimization using a custom-designed method based on mixed integer genetic algorithm.* Engineering Applications of Artificial Intelligence, 2018. **72**: p. 203-212.
11. Fan, X., et al., *Multi-objective optimization for the proper selection of the best heat pump technology in a fuel cell-heat pump micro-CHP system.* Energy Reports, 2020. **6**: p. 325-335.
12. Yanda, L., Z. Yuwei, and N. Razmjooy, *Optimal Arrangement of a Micro-CHP System in the Presence of Fuel Cell-Heat Pump based on Metaheuristics.* International Journal of Ambient Energy, 2020(just-accepted): p. 1-24.
13. Payne, R., J. Love, and M. Kah, *Generating electricity at 60% electrical efficiency from 1-2 kWe SOFC products.* ECS Transactions, 2009. **25**(2): p. 231.
14. Rossi, I., A. Traverso, and D. Tucker, *SOFC/Gas Turbine Hybrid System: A simplified framework for dynamic simulation.* Applied energy, 2019. **238**: p. 1543-1550.
15. Ehyaei, M.A. and M.A. Rosen, *Optimization of a triple cycle based on a solid oxide fuel cell and gas and steam cycles with a multiobjective genetic algorithm and energy, exergy and economic analyses.* Energy conversion and management, 2019. **180**: p. 689-708.
16. Habibollahzade, A., E. Gholamian, and A. Behzadi, *Multi-objective optimization and comparative performance analysis of hybrid biomass-based solid oxide fuel cell/solid oxide electrolyzer cell/gas turbine using different gasification agents.* Applied Energy, 2019. **233**: p. 985-1002.
17. Choudhary, T. and M.K. Sahu, *Energy and exergy analysis of solid oxide fuel cell integrated with gas turbine cycle—"A Hybrid Cycle"*, in *Renewable Energy and its Innovative Technologies*. 2019, Springer. p. 139-153.
18. Ding, X., X. Lv, and Y. Weng, *Coupling effect of operating parameters on performance of a biogas-fueled solid oxide fuel cell/gas turbine hybrid system.* Applied Energy, 2019. **254**: p. 113675.
19. Behzadi, A., et al., *Multi-objective optimization of a hybrid biomass-based SOFC/GT/double effect absorption chiller/RO desalination system with CO2 recycle.* Energy conversion and management, 2019. **181**: p. 302-318.
20. Wang, X., X. Lv, and Y. Weng, *Performance analysis of a biogas-fueled SOFC/GT hybrid system integrated with anode-combustor exhaust gas recirculation loops.* Energy, 2020. **197**: p. 117213.
21. Gong, W. and N. razmjooy, *A new optimisation algorithm based on OCM and PCM solution through energy reserve.* International Journal of Ambient Energy, 2020: p. 1-14.
22. Yin, Z. and N. Razmjooy, *PEMFC identification using deep learning developed by improved deer hunting optimization algorithm.* International Journal of Power and Energy Systems, 2020. **40**(2).
23. Cao, Y., et al., *Experimental modeling of PEM fuel cells using a new improved seagull optimization algorithm.* Energy Reports, 2019. **5**: p. 1616-1625.
24. Holman, J.P., *Heat transfer*. 2002: McGraw-Hill Science, Engineering & Mathematics.
25. Sanaye, S. and H. Hajabdollahi, *Thermal-economic multi-objective optimization of plate fin heat exchanger using genetic algorithm.* Applied Energy, 2010. **87**(6): p. 1893-1902.
26. Bavarsad, P.G., *Energy and exergy analysis of internal reforming solid oxide fuel cell–gas turbine hybrid system.* International journal of hydrogen energy, 2007. **32**(17): p. 4591-4599.
27. Chan, S., H. Ho, and Y. Tian, *Modelling of simple hybrid solid*

oxide fuel cell and gas turbine power plant. Journal of power sources, 2002. **109**(1): p. 111-120.
28. Zhang, G., C. Xiao, and N. Razmjooy, *Optimal Parameter Extraction of PEM Fuel Cells by Meta-heuristics.* International Journal of Ambient Energy, 2020(just-accepted): p. 1-22.
29. Guo, Y., et al., *An optimal configuration for a battery and PEM fuel cell-based hybrid energy system using developed Krill herd optimization algorithm for locomotive application.* Energy Reports, 2020. **6**: p. 885-894.
30. Yuan, Z., et al., *A new technique for optimal estimation of the circuit-based PEMFCs using developed Sunflower Optimization Algorithm.* Energy Reports, 2020. **6**: p. 662-671.
31. Cao, Y., et al., *Multi-objective optimization of a PEMFC based CCHP system by meta-heuristics.* Energy Reports, 2019. **5**: p. 1551-1559.
32. Yu, D., et al., *System identification of PEM fuel cells using an improved Elman neural network and a new hybrid optimization algorithm.* Energy Reports, 2019. **5**: p. 1365-1374.
33. Cuneo, A., et al., *Gas turbine size optimization in a hybrid system considering SOFC degradation.* Applied Energy, 2018. **230**: p. 855-864.
34. Arsalis, A. and G.E. Georghiou, *Thermoeconomic Optimization of a Hybrid Photovoltaic-Solid Oxide Fuel Cell System for Decentralized Application.* Applied Sciences, 2019. **9**(24): p. 5450.
35. Hajilounezhad, T., S. Safari, and M. Aliehyaei, *Multi-Objective Optimization of Solid Oxide Fuel Cell/GT Combined Heat and Power System: A comparison between Particle Swarm and Genetic Algorithms.* 2020.
36. Hosseini Firouz, M. and N. Ghadimi, *Optimal preventive maintenance policy for electric power distribution systems based on the fuzzy AHP methods.* Complexity, 2016. **21**(6): p. 70-88.
37. Leng, H., et al., *A new wind power prediction method based on ridgelet transforms, hybrid feature selection and closed-loop forecasting.* Advanced Engineering Informatics, 2018. **36**: p. 20-30.
38. Liu, Y., W. Wang, and N. Ghadimi, *Electricity load forecasting by an improved forecast engine for building level consumers.* Energy, 2017. **139**: p. 18-30.
39. Lazzaretto, A. and A. Toffolo, *Energy, economy and environment as objectives in multi-criterion optimization of thermal systems design.* Energy, 2004. **29**(8): p. 1139-1157.
40. Calise, F., et al., *Single-level optimization of a hybrid SOFC–GT power plant.* Journal of Power Sources, 2006. **159**(2): p. 1169-1185.
41. Zhao, W., Z. Zhang, and L. Wang, *Manta ray foraging optimization: An effective bio-inspired optimizer for engineering applications.* Engineering Applications of Artificial Intelligence, 2020. **87**: p. 103300.
42. Yang, D., G. Li, and G. Cheng, *On the efficiency of chaos optimization algorithms for global optimization.* Chaos, Solitons & Fractals, 2007. **34**(4): p. 1366-1375.
43. Rim, C., et al., *A niching chaos optimization algorithm for multimodal optimization.* Soft Computing, 2018. **22**(2): p. 621-633.
44. Rashedi, E., H. Nezamabadi-Pour, and S. Saryazdi, *GSA: a gravitational search algorithm.* Information sciences, 2009. **179**(13): p. 2232-2248.
45. Gandomi, A.H. and A.H. Alavi, *Krill herd: a new bio-inspired optimization algorithm.* Communications in Nonlinear Science and Numerical Simulation, 2012. **17**(12): p. 4831-4845.
46. Askarzadeh, A., *A novel metaheuristic method for solving constrained engineering optimization problems: crow search algorithm.* Computers & Structures, 2016. **169**: p. 1-12.
47. Yapici, H. and N. Cetinkaya, *A new meta-heuristic optimizer: Pathfinder algorithm.* Applied Soft Computing, 2019. **78**: p. 545-568.
48. Campanari, S., *Full load and part-load performance prediction for integrated SOFC and microturbine systems.* J. Eng. Gas Turbines Power, 2000. **122**(2): p. 239-246.
49. Leal, E.M., L.A. Bortolaia, and A.M.L. Junior, *Technical analysis of a hybrid solid oxide fuel cell/gas turbine cycle.* Energy Conversion and Management, 2019. **202**: p. 112195.
50. Abrassi, A., et al., *Impact of Different Volume Sizes on Dynamic Stability of a Gas Turbine-Fuel Cell Hybrid System.* Journal of Engineering for Gas Turbines and Power, 2020. **142**(5).
51. Akroot, A., L. Namli, and H. Ozcan, *Compared Thermal Modeling of Anode-and Electrolyte-Supported SOFC-Gas Turbine Hybrid Systems.* Journal of Electrochemical Energy Conversion and Storage, 2020. **18**(1).
52. Barzegar Avval, H., et al., *Thermo-economic-environmental multiobjective optimization of a gas turbine power plant with preheater using evolutionary algorithm.* International Journal of Energy Research, 2011. **35**(5): p. 389-403.